Molecular and Nanostructural Mechanisms of Deformation, Strength and Toughness of Spider Silk Fibrils

Andrea Nova,[†,‖] Sinan Keten,[†] Nicola M. Pugno,[†,⊥,#,∇] Alberto Redaelli,[‖] and Markus J. Buehler*,[†,‡,§,⊥]

[†]Laboratory for Atomistic and Molecular Mechanics, Department of Civil and Environmental Engineering, [‡]Center for Materials Science and Engineering, and [§]Center for Computational Engineering, Massachusetts Institute of Technology, 77 Massachusetts Avenue, Cambridge, Massachusetts 02139, [‖]Department of Bioengineering, Politecnico di Milano, P.zza Leonardo da Vinci 32, 20133, Milano, Italy, [⊥]Laboratory of Bio-Inspired Nanomechanics "Giuseppe Maria Pugno", Department of Structural Engineering and Geotechnics, Politecnico di Torino, Corso Duca degli Abruzzi 24, 10129, Torino, Italy, [#]National Institute of Nuclear Physics (INFN), National Laboratories of Frascati, Via E. Fermi 40, 00044, Frascati, Italy, and [∇]National Institute of Metrological Research (INRIM), Strada delle Cacce 91, I-10135, Torino, Italy

ABSTRACT Spider dragline silk is one of the strongest, most extensible and toughest biological materials known, exceeding the properties of many engineered materials including steel. Silk features a hierarchical architecture where highly organized, densely H-bonded beta-sheet nanocrystals are arranged within a semiamorphous protein matrix consisting of 3_1-helices and beta-turn protein structures. By using a bottom-up molecular-based approach, here we develop the first spider silk mesoscale model, bridging the scales from Angstroms to tens to potentially hundreds of nanometers. We demonstrate that the specific nanoscale combination of a crystalline phase and a semiamorphous matrix is crucial to achieve the unique properties of silks. Our results reveal that the superior mechanical properties of spider silk can be explained solely by structural effects, where the geometric confinement of beta-sheet nanocrystals, combined with highly extensible semiamorphous domains, is the key to reach great strength and great toughness, despite the dominance of mechanically inferior chemical interactions such as H-bonding. Our model directly shows that semiamorphous regions govern the silk behavior at small deformation, unraveling first when silk is being stretched and leading to the large extensibility of the material. Conversely, beta-sheet nanocrystals play a significant role in defining the mechanical behavior of silk at large-deformation. In particular, the ultimate tensile strength of silk is controlled by the strength of beta-sheet nanocrystals, which is directly related to their size, where small beta-sheet nanocrystals are crucial to reach outstanding levels of strength and toughness. Our results and mechanistic insight directly explain recent experimental results, where it was shown that a significant change in the strength and toughness of silk can be achieved solely by tuning the size of beta-sheet nanocrystals. Our findings help to unveil the material design strategy that enables silk to achieve superior material performance despite simple and inferior material constituents. This concept could lead to a new materials design paradigm, where enhanced functionality is not achieved using complex building blocks but rather through the utilization of simple repetitive constitutive elements arranged in hierarchical structures from nano to macro.

KEYWORDS Nanomechanics, biological material, spider silk, protein, H-bond, nanostructure

Spider silk is a strong and tough fibrous biological protein material with a hierarchical structure (Figure 1a) that has evolved to fulfill multiple functions of efficiently storing and dissipating mechanical energy,[1−5] making it one of the toughest and most versatile materials known.[2,6] Silks belong to the broader class of biological structures that have evolved as critical material components in biological systems to provide structural support, force generation, catalytic properties, or energy conversion.[4,7−9] From a biological point of view, spiders take advantage of these unique mechanical features when using silk threads to support their own weight and to absorb kinetic energy to capture prey.[1] From an engineering perspective, silk has been utilized in various technological fields including parachutes, medical sutures, and more recently, tissue regeneration and many other biomedical applications.[10]

Experimental and computational investigations of the structure of silk at the nanoscale revealed that there exist two fundamental structural constituents: highly organized antiparallel beta-sheet nanocrystals and a semiamorphous phase that consists of less orderly protein structures (Figure 1a).[11−13] It has been suggested that the antiparallel beta-sheet nanocrystals[14−16] play a key role in defining silk mechanical properties, as they provide stiff orderly cross-linking domains embedded in a semiamorphous matrix that consists of less orderly beta-structures, 3_1 helices and beta-turns.[11,17,18] Similar to their role in other mechanical proteins,[19−25] it has been hypothesized that H-bond arrays in beta-sheet nanocrystals reinforce the polymeric network
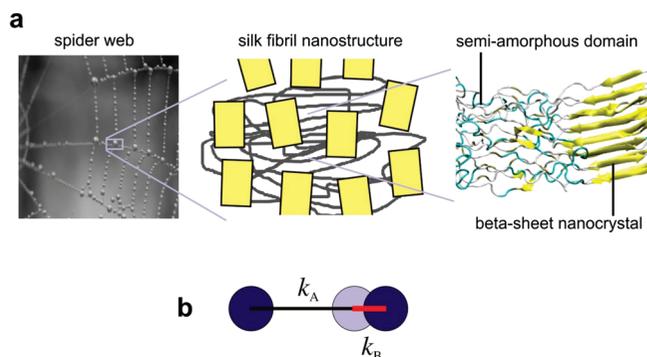
FIGURE 1. Hierarchical structure of spider silk and model formulation. (a) Hierarchical structure of spider silk. The nanostructure of silk fibrils consists of two major constituents, a semiamorphous region and beta-sheet nanocrystals. The focus of this study is the representation of the structure of spider silk through a mesoscale level model, where beta-sheet nanocrystals embedded in a soft matrix are described based on a coarse-grained approach. (b) Representation of a spider silk mesoscale structure using the coarse-grained model. The model consists of a serial arrangement of a crystalline and a semiamorphous region, thereby representing the fundamental unit building block of the silk nanostructure shown in panel a. The mechanical characteristic of each constituting phase is informed from atomistic level molecular dynamics simulations.

FIGURE 2. Constitutive behavior of the two elements represented in the coarse-grained model of silk (obtained from full atomistic molecular dynamics simulation results as reported in refs 14, 29, and 30). (a) Mechanical behavior of the glycine rich semiamorphous domain as reported in ref 30 consisting of three regimes (A, homogeneous stretching of the protein structure; B, onset of yielding and unraveling of the semiamorphous domains via the breaking of H-bonds; C, stretching of protein backbone). (b) Mechanical behavior of beta-sheet nanocrystals under lateral loading. The smallest beta-sheet nanocrystal size (3 nm) shows the characteristic stick—slip phenomenon due to repeated breaking and reformation of H-bonds (modeled here as an elastic-plastic yielding behavior), a phenomenon that is not observed in larger beta-sheet nanocrystals. Larger beta-sheet nanocrystals (>3 nm) show a more brittle and at the same time weaker and softer mechanical behavior as shown in ref 14), reflected in the constitutive behavior shown in panel b.

under mechanical stretch, by forming interlocking regions that transfer the load between chains.[17,26] In particular, Termonia's pioneering empirical two-phase model based on experimental data has been instrumental in explaining the importance of the ratio and size of crystalline and semiamorphous domains, at a time when large-scale atomistic simulations of spider silk constituents were impossible due to the lack of suitable force fields and computational resources.[26] More recently, macroscale experiments demonstrated that when the size of beta-sheet nanocrystals is reduced by moderating the reeling speed or by infiltration, silk displays enhanced toughness and greater ultimate strength,[26–28] exceeding that of steel and other engineered materials.

However, despite progress in experimental, theoretical, and computational studies, thus far no model exists that enables a rigorous understanding of the role of the two fundamental constituents of silk at the intermediate, "composite" level (i.e., the silk fibril nanostructure as shown in Figure 1a). This progress has partly been hindered due to a lack of appropriate atomistic models of silks, and a lack of a thorough understanding of the mechanical behavior of silk's constituents at the nanoscale. Both issues have recently been addressed through protein structure identification methods and large-scale molecular simulation studies, where the molecular structure and mechanical signature of the two key constituents of silks have been identified.[14,29,30] As a result, we are now in a position to understand the fundamentals of the origin of silk's unique material properties directly from an atomistic level and without the need to introduce experimental parameters, an issue that will be addressed in this article. The aim of this work is to utilize key material and structural parameters from atomistic calculations on dragline

silk constituents and to develop a fundamental understanding of silk's exceptional performance by linking the molecular structure and mechanisms to its larger-scale mechanical behavior.

Results and Discussion. To provide a fundamental description of spider silk mechanics from a bottom-up perspective, and to elucidate the design strategy behind the making of silks, here we use a simple coarse-grained model whose parameters are directly informed from atomistic simulation results. A schematic of the model setup is depicted in Figure 1b, showing how a simple combination of beta-sheet nanocrystal and semi-amorphous region is modeled by beads connected via multilinear springs in a serial arrangement. This ensemble represents the silk unit cell and reflects the geometry of silk's nanostructure shown in Figure 1a. Each constituent has a mechanical signature informed from full atomistic simulation[14,29,30] as illustrated in Figure 2 (for details on the model development and setup, see Materials and Methods). This model, albeit extremely simple, is capable of describing the key features of the nanomechanics of spider silk without the introduction of any experimental parameter.
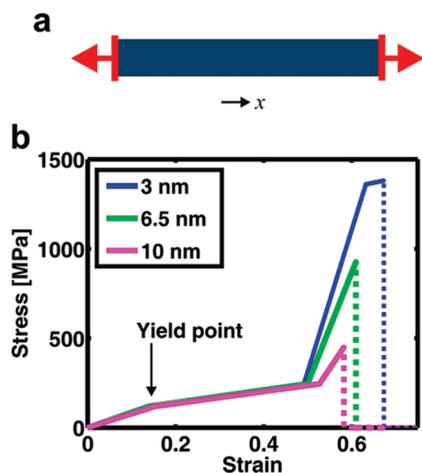
FIGURE 3. Stress—strain response of a silk fibril under tensile loading for varying beta-sheet nanocrystal size. (a) Schematic of model setup and loading geometry of tensile testing. (b) Stress—strain response of spider silk based on different beta-sheet nanocrystal sizes, ranging from 3 to 10 nm. The behavior after rupture has occurred is displayed with dotted lines. The results reveal a remarkable dependence of the stress—strain response on the beta-sheet nanocrystal size. Overall, the stress—strain behavior observed here is in good agreement with experimental results.

We apply the model to simulate the mechanical deformation of silk according to the tensile loading condition shown in Figure 3a. We begin our analysis by considering a system characterized by a beta-sheet nanocrystal size of 3 nm, which corresponds to the size found in natural silk. We find that the resulting stress—strain curve shown in Figure 3b displays the characteristic shape observed in silk, that is, it displays an early yield point, leading to a significant softening and followed by a severe stiffening effect. A detailed analysis reveals that the initial regime is characterized by a relatively high tangent modulus (830 MPa), owing to the homogeneous stretching of semiamorphous regions that are rich in hydrogen bonding in the form of 3_1-helices and beta-turns.[1,11,26] The onset of rupture of the hydrogen bonds in the semiamorphous domains leads to yielding at strain values of around 13% and is evident from a sudden drop in the tangent stiffness. The tangent modulus of this softer regime is much lower, around 310 MPa. During this plateau regime, protein chains in the semiamorphous region gradually unravel along the pulling direction,[27,31] a mechanism that is mediated by the hidden length of the polypeptide that is released as hydrogen bonds break. At a strain value of around 50%, the stress—strain curve enters a high-stiffness regime (with a much higher tangent stiffness of around 8 GPa). At this point, the semiamorphous region has been completely stretched out and the beta-sheet nanocrystal begins to sustain larger strains. An interesting event observed in the stress—strain plot is a short softening regime starting at around 63% strain, immediately prior to failure. A detailed analysis of this phenomenon shows that this is due to the stick—slip failure mechanism of the beta-sheet nanocrystals, a mechanism first described in ref 14. This final high-stress regime contributes significantly to the overall toughness, as it accounts for ap-

proximately 20% of the total energy dissipated before failure. When the applied force reaches the maximum tensile strength at strain values of 67%, individual beta-strands are completely pulled out, and failure occurs at a stress of 1379 MPa. This maximum stress level, on the order of GPa, is in quantitative agreement with results from experimental studies.[27]

We now consider a systematic variation of the beta-sheet nanocrystal size of up to 10 nm and study its impact on silk mechanical properties, with the aim to quantify the effect of the crystal size on the overall mechanical behavior. The motivation for this analysis is to examine earlier hypotheses, suggesting that small changes in crystal size translate altogether into a different overall mechanical response of spider silk.[14,27] The results of the mechanical analysis are shown in Figure 3b, where we plot the stress—strain curves for varying beta-sheet nanocrystal sizes. The most important finding is the observation that the size of beta-sheet nanocrystals, at otherwise completely identical conditions, severely affects the mechanical response. The analysis reported in Figure 3b clearly shows that larger-crystal systems (i.e., 6.5 and 10 nm beta-sheet nanocrystals) have a behavior that deviates significantly from the reference (3 nm) small-crystal case, especially at high levels of deformation. Silk fibrils with larger beta-sheet nanocrystals break at significantly lower stress values, and also show a shorter (61 and 58% strain, respectively) and much softer third regime, with a tangent modulus of 6 and 3.6 GPa, respectively. The initial and intermediate regimes, however, are comparable to the 3 nm crystal case where the transition points and stiffness values do not vary substantially between the two systems.

Our results demonstrate that an increase in beta-sheet nanocrystal size leads to a significant loss of strength and toughness of the system (Figure 4). As shown in Figure 4a, with a value of 925 MPa the 6.5 nm-crystal case shows a decrease in maximum stress of approximately 33% with respect to the reference case. The drop is even larger for the 10 nm crystal case, which fails at 447 MPa, 67% less than the reference case. The drop in maximum stress also leads to a considerably lower toughness value (Figure 4b), with a decrease of 43 and 60% (for the 6.5 and 10 nm cases, respectively) when compared to the reference small beta-sheet nanocrystal case.

We now analyze the deformation mechanisms at different strain levels and for varying beta-sheet nanocrystal size. Figure 5 shows the relative contribution $\Delta L_i/\Delta L_T$ of the semiamorphous domain and of the beta-sheet nanocrystal to the overall deformation and for all the three beta-sheet nanocrystal sizes considered in this study. In the smallest-crystal system (3 nm), the deformation of the beta-sheet nanocrystal starts to play a significant role once the semiamorphous region begins to stiffen at around 50% strain, and clearly dominates deformation when the stick—slip mechanisms of the beta-sheet nanocrystal is triggered (Figure 5a). This increase in beta-sheet nanocrystal deformation at large strains has been hypothesized in earlier experimen-
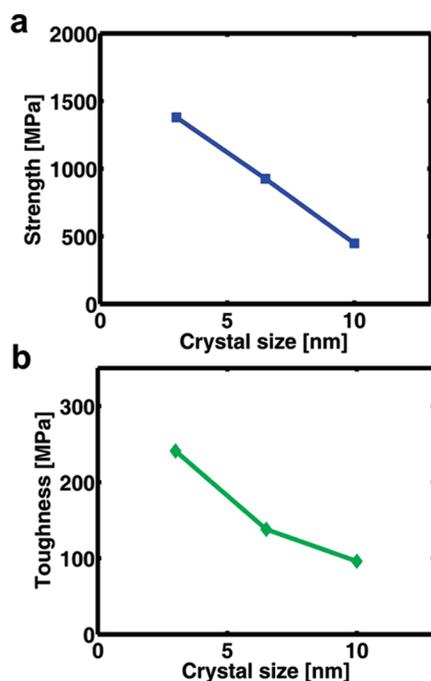
FIGURE 4. Variation of strength and toughness with beta-sheet nanocrystal size. (a) Variation of strength with beta-sheet nanocrystal size. The plot illustrates that silk fibers employing larger beta-sheet nanocrystals have a diminished strength of 925 and 447 MPa for the 6.5 and 10 nm crystal cases, compared with the small-crystal (3 nm) system, which breaks at 1379 MPa. (b) Variation in the toughness (toughness modulus) of the silk constitutive unit as a function of beta-sheet nanocrystal size. Enhanced mechanical properties of small beta-sheet nanocrystals play a governing role in the overall behavior. An increase in the toughness (modulus) from 96 to 138 MPa and 241 MPa is observed when beta-sheet nanocrystal size is reduced from 10 to 6.5 nm and 3 nm.

tal studies, but is here for the first time shown from a molecular perspective and with a direct link to underlying molecular mechanisms. In the larger crystal cases of 6.5 and 10 nm, however, the beta-sheet nanocrystal contribution to deformation reaches significant levels even at small deformation (Figure 5b,c). The reason is a much softer behavior of the beta-sheet nanocrystals (as illustrated in Figure 2b), which results in greater displacements of the nanocrystal domain. This observation demonstrates the importance of the great stiffness of beta-sheet nanocrystals to enable the specific deformation mechanisms that are crucial to silk's mechanical properties.

Next we compare the maximum deformation of the semiamorphous region at the failure point, for different beta-sheet nanocrystal sizes. As shown in Figure 6, we observe that the semiamorphous regions are less stretched in systems with larger beta-sheet nanocrystals. The maximum strain $\Delta L_A / \Delta L_{A,0}$ reached in the semiamorphous region is 61% in the 3 nm beta-sheet nanocrystal case, 56% in the 6.5 nm case, and around 51% in the 10 nm case. This is an important observation, which suggests that the increase in the beta-sheet nanocrystal size prevents the material to take full advantage of the entire potential of the semiamorphous region, that is, to unravel its hidden length and thus severely
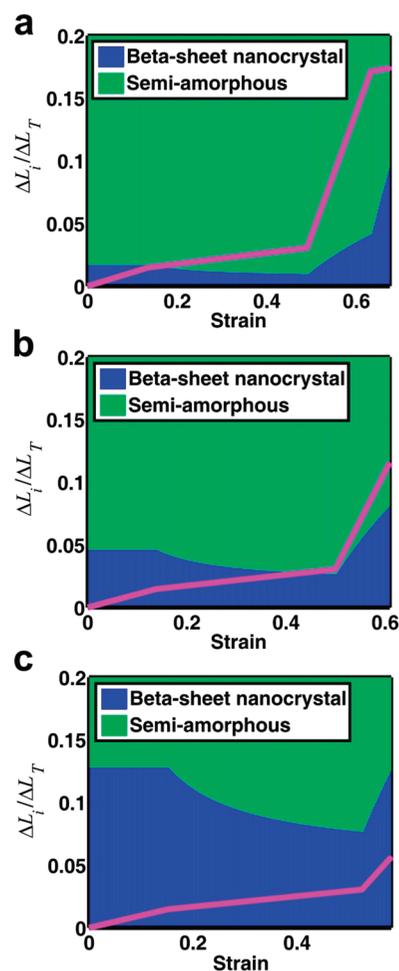
FIGURE 5. Deformation mechanisms of silk constitutive elements, as a function of beta-sheet nanocrystal size (3 nm in panel a, 6.5 nm case in panel b, and 10 nm in c). The plot shows the relative contribution of beta-sheet nanocrystal deformation and deformation of the semiamorphous region as a function of strain. (a) Since the beta-sheet nanocrystal is much stiffer than the semiamorphous phase, its contribution to the total deformation is initially small. The softening of the semiamorphous phase results in an even smaller contribution for the beta-sheet nanocrystal as deformation is increased. However, when the semiamorphous region enters the stiff covalent regime, the beta-sheet nanocrystals deform more significantly. The final regime with a drastic drop in beta-sheet nanocrystal properties due to stick−slip phenomena is associated with a noticeable increase of beta-sheet nanocrystal stretching, finally leading to failure of the system. This panel illustrates that beta-sheet nanocrystals contribute to deformation primarily in the final stages of deformation. (b,c) Since the larger beta-sheet nanocrystals are less stiff, their contribution to deformation is larger than in the small beta-sheet nanocrystal case (panel a). Note that the data shown is zoomed into 20% on the y-axis to focus on the range of contributions of the beta-sheet nanocrystals more clearly.

affecting silk's extensibility and energy dissipation capacity as is evident from the data shown in Figure 4.[32,33]

Overall, the results of our study are in excellent agreement with experimental data, where a similar variation of the beta-sheet nanocrystal size and its impact on larger-scale mechanical properties was reported recently,[27] showing a drastic drop in toughness when beta-sheet nanocrystal size increases (in experiments,[27] the change in the beta-sheet
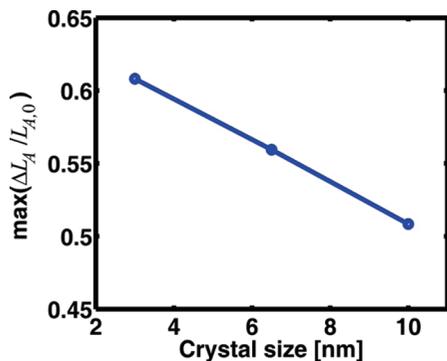
FIGURE 6. Deformation of semiamorphous region in silk, as a function of beta-sheet nanocrystal size. The analysis reveals that larger beta-sheet nanocrystals prohibit the semiamorphous region from fully extending, reducing the energy dissipation capacity of the material. In the 10 nm case, the semiamorphous region deforms only up to around 51% its initial length, while it can reach values of 56 and 61% in the 6.5 and 3 nm cases.

nanocrystal size was achieved via a change of the reeling speed, showing a drop of strength from approximately 1500 to 300 MPa as the beta-sheet nanocrystal size was increased, in reasonable agreement with the results shown in Figure 4a). We note that the failure strain values in the three systems that we investigated here are larger than those found in experimental studies (between 10 and 50% more). This phenomenon can be explained based on two points. First, in our model we consider an ideal and rather simplified (one-dimensional) model that completely lacks statistical variability and structural defects. This generally leads to enhanced strength and extensibility in comparison to systems with defects (as is likely the case for experimental results). Second, we underline that physiologically spun silks (i.e., the small-crystal case) undergo a substantial prestretching at the orifice.[27,34] However, the current model does not include this effect and we consequently expect an overestimation of the stretching capacity of the material. Future models could directly include variability of structure and defects in silk and model the effect of prestretching to allow a better comparison with experimental data. This could, for example, be achieved by the development of a two/three-dimensional model of silk fibrils.

Conclusion. The most important finding of our study is that it has revealed the mechanistic interplay of the two constitutive phases of silk, semiamorphous regions and highly organized beta-sheet nanocrystals, as well as the effect of structural changes on the overall mechanical behavior of silk. We find that semiamorphous regions unravel first when silk is being stretched, leading to its large extensibility. Conversely, the large-deformation mechanical properties and ultimate tensile strength of silk are controlled by the strength of beta-sheet nanocrystals, which is directly related to their size. An important discovery is that small beta-sheet nanocrystals are crucial to reach outstanding levels of strength and toughness, as shown clearly in Figures 3−5. A key observation from our study is that the unraveling of semiamorphous regions is severely influ-

enced by the size of the beta-sheet nanocrystals (Figure 6), and that only ultrasmall crystals provide the basis for silk to take full advantage of its high extensibility, failure stress, and energy dissipation capacity. Small-crystal systems guarantee the required cross-linking strength that is necessary for the semiamorphous domains to fully extend and to enter a high-stiffness covalent regime, when beta-sheet nanocrystals are being stretched and eventually fail. The resulting capacity to sustain large tensile force as well as extension enhances the strength and energy dissipation ability of the material. Overall, the confinement of beta-sheet nanocrystals to the nanoscale is essential for the superior mechanical properties of silks, as this is crucial to reach high extensibility and high levels of stress. Our results further show that the severe change of the mechanical properties of spider silk under relatively small variations of the size of beta-sheet nanocrystals can be explained solely based on structural effects (Figure 3−4). Our findings also relate the characteristic yielding point in the stress−strain curve, observed universally for many types of silks, to the onset of failure of semiamorphous regions, when H-bonded 3_1-helices and beta-turns begin to rupture (see Figure 2a).

Our findings have impact beyond our understanding of silk mechanics, as they show that by solely controlling the structure at the nanoscale, a tailoring of material properties at the microscale is possible without the need to introduce any new material constituents. This could provide us with a powerful alternative to the traditional engineering top-down approach of shaping materials to obtain specific properties and enable the bottom-up design of complex materials.[35] Thereby, the application of our findings to the design of synthetic materials could provide us with new material concepts based on inexpensive, abundant constituents and facilitate the development of effective cross-linking domains in other materials.[36,37] Technologically, we are not limited by "simple" natural building blocks such as amino acids. Therefore, the incorporation and transfer of the materials design strategies identified here into synthetic materials could result in materials with significantly better performance and much higher levels of strength and toughness, while reaching similar levels of extensibility. The incorporation of mutability concepts could be used to design materials whose mechanical properties can be controlled by external cues such as humidity,[38−40] temperature, pH, magnetic or electric fields by providing a strategy to control the nanostructure of the material and thereby its functional properties.

Materials and Methods. *Coarse-Grained Molecular Model.* A multiscale computational bottom-up investigation of spider silk, the approach employed in this work, is a powerful tool to understand its mechanical properties from a fundamental perspective. At length-scales on the order of hundreds of nanometers, spider silk appears as an entanglement of polypeptide chains with two distinct domains that consist of (A) a semiamorphous region[13,41] and (B) a highly ordered crystalline domain consisting of beta-sheet nanocrystals.[26] We model the silk constitutive unit as a combina-

2630

DOI: 10.1021/nl101341w | *Nano Lett.* **2010,** *10,* 2626–-2634

TABLE 1. Model Parameters for the Semi-Amorphous Region in the Mesoscale Model

model parameter	value
$k_{A,1}$ (pN/Å) - initial regime	9.9
$k_{A,2}$ (pN/Å) - intermediate regime	3.96
$k_{A,3}$ (pN/Å) - final regime	103.84
$\Delta L_{A,1}$ (Å) - first transition point	12.0
$\Delta L_{A,2}$ (Å) - second transition point	43.8
$L_{A,0}$ (Å) - initial length	90.0

TABLE 2. Model Parameters for the Beta-Sheet Nanocrystal in the Mesoscale Model

model parameter	beta-sheet nanocrystal size		
	3 nm crystal	6.5 nm crystal	10 nm crystal
$k_{B,1}$ (pN/Å) - initial stiffness	576	205.5	67.53
$k_{B,2}$ (pN/Å) - second-regime stiffness	5.76	N/A	N/A
$\Delta L_{B,1}$ (Å) - softening point	2.36	N/A	N/A
$\Delta L_{B,2}$ (Å) - breaking point	5.8	4.5	6.63
F_{max} (pN) - maximum tensile strength	1380	925	447
$L_{B,0}$ (Å) - initial length	0	0	0

tion of these two domains, as shown in Figure 1b. The structure and mechanical behavior of these domains have been previously explored by atomistic simulations,[29,30] enabling us to feed a complete set of constitutive parameters directly from lower, molecular scales.

A model made up of a series of springs is a simple, yet powerful way to link nanostructural features and mechanical signatures of constitutive elements to the overall mechanical behavior at the silk-fibril scale. The serial spring assumption is reasonable at the nanoscale, since in the sequence of spider silk the crystalline domains are followed by the glycine-rich repeats that form the semiamorphous regions, resulting in a serial constitutive unit that is the fundamental building block of more complex hierarchies at larger scales.[42]

Model Formulation and Parameter Identification. Full-atomistic simulations to understand the mechanical properties of the two distinct regions of spider silk have been performed in earlier studies.[29,30] A representative volume element containing 15 polypeptide chains is used to derive the constitutive behavior. This approach of considering more than one chain in the atomistic mechanical characterization allows us to obtain a distribution of mechanical responses and to compute their averaged value. When compared to a single-chain mechanical characterization, this approach also accounts for the various interactions between chains within the semiamorphous domain. This is critical, for example, to accurately describe the constitutive properties of 3_1-helices that involve multiple polypeptide chains. The effective force−extension behavior derived from the large molecular assembly is then normalized by the force, area, and length per single polypeptide chain to develop an appropriate constitutive law. The results from these analyses are used directly to determine the parameters of the present coarse-grained model, representing a single amorphous domain and a single beta-sheet nanocrystal.

We approximate the force-displacement behavior of the two constituting phases in silk under tensile loading with a multilinear model. Numerical values of all parameters developed here are given in Tables 1 and 2, and details on the mathematical formulation and parameter identification are given below.

Semiamorphous Region. Atomistic simulations revealed a characteristic three-stage deformation pattern, where an initial stiff regime is followed by a yielding point and a long plateau, and eventual significant stiffening as the polypep-

tide's backbone is being stretched.[29,30] This behavior is associated to the presence and the breaking of secondary structures such as 3_1-helices and beta-turns, which are rich in intrachain and interchain hydrogen bonding.[11,26] At larger strains, the structure enters a final high-stiffness regime, characterized by the stretching of covalent bonds along the protein backbone.

Values for the stiffness of the three different regimes of the semiamorphous domain are extracted from atomistic simulation data.[29,30] By fitting these results with a trilinear function, we obtain the tangent stiffnesses as a function of the displacement, where $\Delta L_A = L_A - L_{A,0}$ describes the deformation of the semiamorphous region (relative to the initial length). The stiffness as a function of deformation is then given by

$$k_A(\Delta L_A) = \begin{cases} k_{A,1} & \Delta L_A < \Delta L_{A,1} \\ k_{A,2} & \Delta L_{A,1} \leq \Delta L_A \leq \Delta L_{A,2} \\ k_{A,3} & \Delta L_A > \Delta L_{A,2} \end{cases} \quad (1)$$

where the values for $k_{A,i}$ as well as the transition deformations $\Delta L_{A,1}$ and $\Delta L_{A,2}$ are summarized in Table 1. The force versus deformation of the amorphous domain is given by the following law

$$F_A(\Delta L_A) = \begin{cases} k_{A,1}\Delta L_A & \Delta L_A < \Delta L_{A,1} \\ k_{A,1}\Delta L_{A,1} + k_{A,2}(\Delta L_A - \Delta L_{A,1}) & \Delta L_{A,1} \leq \Delta L_A \leq \Delta L_{A,2} \\ k_{A,1}\Delta L_{A,1} + k_{A,2}(\Delta L_{A,2} - \Delta L_{A,1}) + & \\ \qquad k_{A,3}(\Delta L_A - \Delta L_{A,2}) & \Delta L_A > \Delta L_{A,2} \end{cases}$$

$$(2)$$

The resulting force-deformation curve of the semiamorphous region is shown in Figure 2a.

Beta-Sheet Nanocrystal. The beta-sheet nanocrystal is modeled as a nonlinear spring, where the force-displacement characteristic is informed from atomistic simulation results.[14,29,30,43,44] The beta-sheet nanocrystal is modeled as two beads superimposed on one another, and the bond between these beads characterizes its mechanical response. From ato-

mistic simulations[14] it was found that the properties of the beta-sheet nanocrystals vary as a function of crystal size, where small crystals are stiffer, dissipate more energy through a stick−slip mechanism and fail at higher force values. We consider the effect of the variation in size of beta-sheet nanocrystals on the mechanical behavior by scaling the crystal stiffness, strength and energy dissipation capacity according to size-effects observed in atomistic simulations. To account for these effects, beta-sheet nanocrystals of different size feature distinct mechanical properties[45−47] in this model.

The beta-sheet crystal stiffness is modeled as a function of the crystal deformation, computed as $\Delta L_B = L_B - L_{B,0}$. The expression for the stiffness k_B as a function of deformation ΔL_B is then given by

$$k_B(\Delta L_B) = \begin{cases} k_{B,1} & \Delta L_B < \Delta L_{B,1} \\ k_{B,2} & \Delta L_B \geq \Delta L_{B,1} \end{cases} \quad (3)$$

where $\Delta L_{B,1}$ is the beta-sheet nanocrystal transition point as defined in Table 2 and shown in Figure 2b.

The force as a function of deformation is given by the following expression

$$F_B(\Delta L_B) =$$
$$H(\Delta L_B)\begin{cases} k_{B,1}\Delta L_B & \text{if } \Delta L_B < \Delta L_{B,1} \\ k_{B,1}\Delta L_{B,1} + k_{B,2}(\Delta L_B - \Delta L_{B,1}) & \text{if } \Delta L_B \geq \Delta L_{B,1} \end{cases}$$
$$(4)$$

where the Heaviside function H is defined as $H(\Delta L_B) = 1$ for $\Delta L_B < L_{B,2}$ and $H(\Delta L_B) = 0$ for $\Delta L_B \geq L_{B,2}$.

The failure point, $\Delta L_{B,2}$ depends on the crystal size as summarized in Table 2. The transition point $\Delta L_{B,1}$, representing the onset of stick−slip motion, only exists in the smallest 3 nm beta-sheet nanocrystal case. For the larger beta-sheet nanocrystals (6.5 and 10 nm cases), the force on the linear spring is simply given as

$$F_B(\Delta L_B) = H(\Delta L_B)k_{B,1}\Delta L_B \quad (5)$$

The spring constants are calculated by dividing the maximum tensile strength by the softening deformation for the 3 nm case and by the breaking point for the larger-crystal cases. The second, softer regime for the small-crystal case is assumed to feature a constant stiffness equal to 1 % of the initial one (see Figure 2b), approximating the stick−slip behavior observed in atomistic simulations through an elastic plastic model.[14] The calculation of the breaking point is done by maintaining the dissipated-energy proportion between beta-sheet nanocrystals of different size. Explicit atomistic simulations suggest that a 3 nm crystal is approximately three times tougher than a 6.5 nm

crystal and in the context of the bilinear spring model[14] this results in a breaking point value of 5.8 Å. We note that the atomistic calculations on strength and effective stiffness are based on the pull-out force required to separate a single strand from the crystal, to be consistent with the normalization for a single polypeptide strand.

The maximum tensile strength of beta-sheet nanocrystals of different size[14] is derived directly from atomistic simulation for the 3 and 6.5 nm beta-sheet nanocrystals,[14] while it is linearly extrapolated for the 10 nm case. To be consistent with the force values of the semiamorphous domain, the maximum strength is directly calculated from simulations in implicit solvent for a 3 nm crystal system, and the large beta-sheet nanocrystal strengths are then determined using the strength ratio from explicit simulations. The softening point for the 3 nm beta-sheet nanocrystal is extracted from explicit simulation results, as well as the breaking point for the 6.5 nm beta-sheet nanocrystal. In the 10 nm case, the breaking point is linearly extrapolated, keeping the same ratio of increase in breaking deformation as in the other two cases (6.5 and 10 nm). Both extrapolations for the 10 nm beta-sheet nanocrystal are performed in order to study a limiting case in the analysis of the effects of crystal size.

Parameter Sensitivity. Since all constitutive elements feature a multilinear elastic behavior, it is possible to predict a linear behavior in the response of the system to a parameter variation, either resulting from a different mechanical signature or from an error in the parameter estimate. Of particular interest is the dependence of the overall strength on the strength of the beta-sheet nanocrystal. Given the fact that the large-deformation behavior (including the fracture behavior) is controlled solely by the beta-sheet nanocrystal phase, a percentage variation in the maximum tensile strength of the beta-sheet nanocrystal correlates directly with the maximum tensile strength of the overall structure.

Model Setup, Computing Technique and Stress Calculation. The MATLAB script provided in Supporting Information is used for calculating the stress−strain behavior of the one-dimensional serial spring model discussed in this work. The effective stiffness of the system under tensile stretch is given by a serial arrangement of two springs and corresponds to

$$k_T(\Delta L_A, \Delta L_B) = \frac{k_A(\Delta L_A)k_B(\Delta L_B)}{k_A(\Delta L_A) + k_B(\Delta L_B)} \quad (6)$$

Force-displacement calculations are carried out by applying displacement increments to the system and computing the relative deformations of the serial springs as a function of their instantaneous stiffness. The displacement of each element can be computed based on eq 6 such that total deformation equals $\Delta L_T = \Delta L_A + \Delta L_B$ at any point, and forces can be evaluated from eqs 2, 4, and 5. Stress values

are derived from force calculations by considering a square cross-sectional area $A = 10 \text{ Å} \times 10 \text{ Å}$ (this estimate for the effective area of a single polypeptide chain is based on a geometric analysis of the spider dragline silk nanostructures obtained in earlier atomistic simulation studies[29,30]) along the whole system length such that $\sigma = F/A$, where σ is the computed stress, F is force per chain and A denotes the cross-sectional area associated with a single polypeptide chain.

Calculation of Toughness. Mechanical toughness is calculated measuring the area under the force−extension curve (until structural failure) by means of a trapezoidal numerical integration.

Note Added after ASAP Publication. There were several changes made to the version of this paper published ASAP June 2, 2010; the corrected version published ASAP June 9, 2010.

Supporting Information Available. Supporting Information is available, containing a Matlab script. This material is available free of charge via the Internet at http://pubs.acs.org.

REFERENCES AND NOTES

(1) Porter, D.; Vollrath, F.; Shao, Z. Predicting the mechanical properties of spider silk as a model nanostructured polymer. *Eur. Phys. J. E* **2005**, *16* (2), 199–206.

(2) Vollrath, F.; Knight, D. P. Liquid crystalline spinning of spider silk. *Nature* **2001**, *410* (6828), 541–548.

(3) Rammensee, S.; Slotta, U.; Scheibel, T.; Bausch, A. R. Assembly mechanism of recombinant spider silk proteins. *Proc. Natl. Acad. Sci. U.S.A.* **2008**, *105* (18), 6590–6595.

(4) Fratzl, P.; Weinkamer, R. Nature's hierarchical materials. *Prog. Mater. Sci.* **2007**, *52*, 1263–1334.

(5) Meyers, M. A.; Chen, P. Y.; Lin, A. Y. M.; Seki, Y. Biological materials: Structure and mechanical properties. *Prog. Mater. Sci.* **2008**, *53* (1), 1–206.

(6) Shao, Z. Z.; Vollrath, F. Materials: Surprising strength of silkworm silk. *Nature* **2002**, *418* (6899), 741–741.

(7) Fratzl, P.; Barth, F. G. Biomaterial systems for mechanosensing and actuation. *Nature* **2009**, *462* (7272), 442–448.

(8) Gao, H.; Ji, B.; Jäger, I. L.; Arzt, E.; Fratzl, P. Materials become insensitive to flaws at nanoscale: Lessons from nature. *P. Natl. Acad. Sci. U.S.A.* **2003**, *100* (10), 5597–5600.

(9) Buehler, M. J.; Keten, S. Failure of molecules, bones, and the earth itself. *Rev. Mod. Phys.* **2010**, *82*, 1459–1487.

(10) Vepari, C.; Kaplan, D. L. Silk as a biomaterial. *Prog. Polym. Sci.* **2007**, *32* (8−9), 991–1007.

(11) van Beek, J. D.; Hess, S.; Vollrath, F.; Meier, B. H. The molecular structure of spider dragline silk: Folding and orientation of the protein backbone. *Proc. Natl. Acad. Sci. U.S.A.* **2002**, *99* (16), 10266–10271.

(12) Lefevre, T.; Rousseau, M. E.; Pezolet, M. Protein secondary structure and orientation in silk as revealed by Raman spectromicroscopy. *Biophys. J.* **2007**, *92* (8), 2885–2895.

(13) Kummerlen, J.; vanBeek, J. D.; Vollrath, F.; Meier, B. H. Local structure in spider dragline silk investigated by two-dimensional spin-diffusion nuclear magnetic resonance. *Macromolecules* **1996**, *29* (8), 2920–2928.

(14) Keten, S.; Xu, Z.; Ihle, B.; Buehler, M. J. Nanoconfinement controls stiffness, strength and mechanical toughness of [beta]-sheet crystals in silk. *Nat. Mater.* **2010**, *9* (4), 359–367.

(15) Fossey, S. A.; Nemethy, G.; Gibson, K. D.; Scheraga, H. A. Conformational Energy Studies of Beta-Sheets of Model Silk Fibroin Peptides 0.1. Sheets of Poly(Ala-Gly) Chains. *Biopolymers* **1991**, *31* (13), 1529–1541.

(16) Xiao, S. B.; Stacklies, W.; Cetinkaya, M.; Markert, B.; Grater, F. Mechanical Response of Silk Crystalline Units from Force-Distribution Analysis. *Biophys. J.* **2009**, *96* (10), 3997–4005.

(17) Hayashi, C. Y.; Shipley, N. H.; Lewis, R. V. Hypotheses that correlate the sequence, structure, and mechanical properties of spider silk proteins. *Int. J. Biol. Macromol.* **1999**, *24* (2−3), 271–275.

(18) Grubb, D. T.; Jelinski, L. W. Fiber morphology of spider silk: The effects of tensile deformation. *Macromolecules* **1997**, *30* (10), 2860–2867.

(19) Rief, M.; Gautel, M.; Oesterhelt, F.; Fernandez, J. M.; Gaub, H. E.; Reversible unfolding of individual titin immunoglobulin domains by, A. F. M. *Science* **1997**, *276* (5315), 1109–1112.

(20) Lee, E. H.; Gao, M.; Pinotsis, N.; Wilmanns, M.; Schulten, K. Mechanical strength of the titin Z1Z2-telethonin complex. *Structure (London)* **2006**, *14* (3), 497–509.

(21) Marszalek, P. E.; Lu, H.; Li, H. B.; Carrion-Vazquez, M.; Oberhauser, A. F.; Schulten, K.; Fernandez, J. M. Mechanical unfolding intermediates in titin modules. *Nature* **1999**, *402* (6757), 100–103.

(22) Brockwell, D. J.; Paci, E.; Zinober, R. C.; Beddard, G. S.; Olmsted, P. D.; Smith, D. A.; Perham, R. N.; Radford, S. E. Pulling geometry defines the mechanical resistance of a beta-sheet protein. *Nat. Struct. Biol.* **2003**, *10* (9), 731–737.

(23) Eom, K.; Li, P. C.; Makarov, D. E.; Rodin, G. J. Relationship between the mechanical properties and topology of cross-linked polymer molecules: Parallel strands maximize the strength of model polymers and protein domains. *J. Phys. Chem. B* **2003**, *107* (34), 8730–8733.

(24) Sulkowska, J. I.; Cieplak, M. Mechanical stretching of proteins - a theoretical survey of the Protein Data Bank. *J. Phys.: Condens. Matter* **2007**, *19* (28), xx.

(25) Buehler, M. J.; Yung, Y. C. Deformation and failure of protein materials in physiologically extreme conditions and disease. *Nat. Mater.* **2009**, *8* (3), 175–188.

(26) Termonia, Y. Molecular Modeling of Spider Silk Elasticity. *Macromolecules* **1994**, *27* (25), 7378–7381.

(27) Du, N.; Liu, X. Y.; Narayanan, J.; Li, L. A.; Lim, M. L. M.; Li, D. Q. Design of superior spider silk: From nanostructure to mechanical properties. *Biophys. J.* **2006**, *91* (12), 4528–4535.

(28) Lee, S. M.; Pippel, E.; Gosele, U.; Dresbach, C.; Qin, Y.; Chandran, C. V.; Brauniger, T.; Hause, G.; Knez, M. Greatly Increased Toughness of Infiltrated Spider Silk. *Science* **2009**, *324* (5926), 488–492.

(29) Keten, S.; Buehler, M. J. Atomistic model of the spider silk nanostructure. *Appl. Phys. Lett.* **2010**, *96*, 153701.

(30) Keten, S.; Buehler, M. J. Nanostructure and molecular mechanics of dragline spider silk protein assemblies. *J. R. Soc., Interface* **2010**, doi:10.1098/rsif.2010.0149.

(31) Rousseau, M. E.; Lefevre, T.; Beaulieu, L.; Asakura, T.; Pezolet, M. Study of protein conformation and orientation in silkworm and spider silk fibers using Raman microspectroscopy. *Biomacromolecules* **2004**, *5* (6), 2247–2257.

(32) Fantner, G. E.; Hassenkam, T.; Kindt, J. H.; Weaver, J. C.; Birkedal, H.; Pechenik, L.; Cutroni, J. A.; Cidade, G. A. G.; Stucky, G. D.; Morse, D. E.; Hansma, P. K. Sacrificial bonds and hidden length dissipate energy as mineralized fibrils separate during bone fracture. *Nat. Mater.* **2005**, *4* (8), 612–616.

(33) Hartmann, M. A.; Fratzl, P. Sacrificial Ionic Bonds Need To Be Randomly Distributed To Provide Shear Deformability. *Nano Lett.* **2009**, *9* (10), 3603–3607.

(34) Papadopoulos, P.; Sölter, J.; Kremer, F. Hierarchies in the structural organization of spider silk—a quantitative model. *Colloid Polym. Sci.* **2009**, *287* (2), 231–236.

(35) LeDuc, P. R.; Robinson, D. N. Using Lessons from Cellular and Molecular Structures for Future Materials. *Adv. Mater.* **2007**, *19*, 3761–3770.

(36) Knowles, T. P.; Fitzpatrick, A. W.; Meehan, S.; Mott, H. R.; Vendruscolo, M.; Dobson, C. M.; Welland, M. E. Role of intermolecular forces in defining material properties of protein nanofibrils. *Science* **2007**, *318* (5858), 1900–1903.

(37) Buehler, M. J. Strength in numbers. *Nat. Nanotechnol.* **2010**, *5* (3), 172–174.

(38) Vehoff, T.; Glisovic, A.; Schollmeyer, H.; Zippelius, A.; Salditt, T. Mechanical Properties of Spider Dragline Silk: Humidity, Hysteresis, and Relaxation. *Biophys. J.* **2007**, *93* (12), 4425–4432.

(39) Vollrath, F.; Porter, D. Spider silk as archetypal protein elastomer. *Soft Matter* **2006**, *2* (5), 377–385.

(40) Porter, D.; Vollrath, F. The role of kinetics of water and amide bonding in protein stability. *Soft Matter* **2008**, *4* (2), 328–336.

(41) Michal, C. A.; Jelinski, L. W. Rotational-echo double-resonance in complex biopolymers: a study of Nephila clavipes dragline silk. *J. Biomol. NMR* **1998**, *12* (2), 231–241.

(42) Simmons, A. H.; Michal, C. A.; Jelinski, L. W. Molecular orientation and two-component nature of the crystalline fraction of spider dragline silk. *Science* **1996**, *271* (5245), 84–87.

(43) Keten, S.; Buehler, M. J. Geometric Confinement Governs the Rupture Strength of H-bond Assemblies at a Critical Length Scale. *Nano Lett.* **2008**, *8* (2), 743–748.

(44) Keten, S.; Buehler, M. J. Asymptotic strength limit of hydrogen bond assemblies in proteins at vanishing pulling rates. *Phys. Rev. Lett.* **2008**, *100*, 198301.

(45) Philip, M. C.; Stephen, A. F.; Margaret, A. A.; John, W. S.; David, L. K.; Adams, W. W.; Ronald, K. E.; David, M.; Deborah, L. V. Mechanical and thermal properties of dragline silk from the spider Nephila clavipes. *Polym. Adv. Technol.* **1994**, *5* (8), 401–410.

(46) Oroudjev, E.; Soares, J.; Arcidiacono, S.; Thompson, J. B.; Fossey, S. A.; Hansma, H. G. Segmented nanofibers of spider dragline silk: Atomic force microscopy and single-molecule force spectroscopy. *Proc. Nat. Acad. Sci. U.S.A* **2002**, *99* (90002), 6460–6465.

(47) Krasnov, I.; Diddens, I.; Hauptmann, N.; Helms, G.; Ogurreck, M.; Seydel, T.; Funari, S. S.; Muller, M. Mechanical properties of silk: Interplay of deformation on macroscopic and molecular length scales. *Phys. Rev. Lett.* **2008**, *100* (4), No. 048104.